Centrum voor Wiskunde en Informatica

REPORT*RAPPORT*

MAS

Modelling, Analysis and Simulation

Modelling, Analysis and Simulation

Riemann-problem and level-set approaches for two-fluid flow computations
I. Linearized Godunov scheme

B. Koren, M.R. Lewis, E.H. van Brummelen, B. van Leer

REPORT MAS-R0112 AUGUST 2001

CWI is the National Research Institute for Mathematics and Computer Science. It is sponsored by the Netherlands Organization for Scientific Research (NWO).
CWI is a founding member of ERCIM, the European Research Consortium for Informatics and Mathematics.

CWI's research has a theme-oriented structure and is grouped into four clusters. Listed below are the names of the clusters and in parentheses their acronyms.

Probability, Networks and Algorithms (PNA)

Software Engineering (SEN)

Modelling, Analysis and Simulation (MAS)

Information Systems (INS)

P.O. Box 94079, 1090 GB Amsterdam (NL)
Kruislaan 413, 1098 SJ Amsterdam (NL)
Telephone +31 20 592 9333
Telefax +31 20 592 4199

ISSN 1386-3703

Riemann-Problem and Level-Set Approaches for Two-Fluid Flow Computations I. Linearized Godunov Scheme

B. Koren, M.R. Lewis and E.H. van Brummelen
CWI
P.O. Box 94079, 1090 GB Amsterdam, The Netherlands

B. van Leer
The University of Michigan, Department of Aerospace Engineering
Ann Arbor, MI 48109-2140, USA

ABSTRACT
A finite-volume method is presented for the computation of compressible flows of two immiscible fluids at very different densities. The novel ingredient in the method is a two-fluid linearized Godunov scheme, allowing for flux computations in case of different fluids (e.g., water and air) left and right of a cell face. A level-set technique is employed to distinguish between the two fluids. The level-set equation is incorporated into the system of hyperbolic conservation laws.

2000 Mathematics Subject Classification: 65M60, 76N99, 76T10
Keywords and Phrases: free surfaces, compressible liquid-gas flows, interface capturing, Godunov scheme, level-set method.
Note: This research was supported by the Dutch Technology Foundation STW (applied science division of NWO and the technology programme of the Ministry of Economic Affairs) and by the Maritime Research Institute Netherlands. The work was carried out under CWI-project MAS2.1 "Computational Fluid Dynamics".

1. Introduction

1.1 Application area: water-air flows

The present paper is directed towards the computation of two-fluid flows consisting of water and air. Premises are that the water and air do not mix and that vaporization and condensation phenomena do not occur. Furthermore, the surface water waves that are of practical relevance are assumed to be of sufficiently large scale to safely neglect surface tension. Despite these simplifications, the application area is still vast: computational ship hydrodynamics, the combined computation of wind fields and sea currents, etc. Various computational challenges exist in accurately and efficiently computing water-air flows, in particular their interfaces.

1.2 Treatment of free-surface flows

1.2.1 Basic grid techniques To compute a free surface on a grid, basically two techniques exist: (i) moving or fitting (Lagrangean) techniques and (ii) fixed-grid (Eulerian) techniques. In the first, the free surface forms (part of) the grid boundary (Figure 1a); the latter is fit to the free surface. In the second, the free surface is in general not aligned with the grid (Figure 1b). Because in the moving-grid approach the grid is attached to the free boundary, its free surface is crisp, but it is not necessarily accurate; its location and topology may be poorly resolved. A moving-grid technique is not well-suited for the computation of bifurcating free surfaces. In practice, it may even be unsuited for free surfaces that are non-bifurcating, but just strongly distorted. Fixed-grid techniques do not suffer from such drawbacks, but here the front may be diffused. Mixed Lagrangean-Eulerian methods,

which try to combine the best of the above two basic techniques, may be constructed. An example of such a hybrid approach would be to overlay a fixed grid with a narrow moving grid attached to the free surface (Figure 1c). We proceed by considering moving- and fixed-grid techniques in more detail.

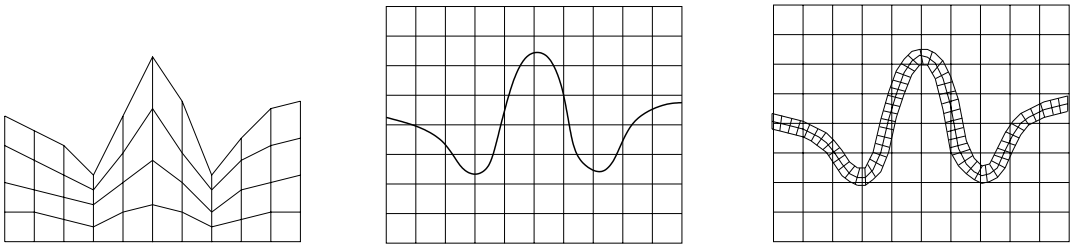

a. Moving b. Fixed c. Hybrid

Figure 1: Types of grid techniques for computing free-surface flows.

1.2.2 Moving-grid techniques A common approach in moving-grid techniques is to describe the free surface as a height function, say as $h(x,t)$ in the 2D unsteady case (Figure 2), or as $h(x,y,t)$ in 3D. Some references to free-surface height methods are [1, 2, 3]. It is common use to do the calculation of the free-surface height separately from that of the bulk flow, a reason being that in case of a single-valued height function, the free-surface-flow problem is one dimension lower than the bulk-flow problem. (Methods that compute the height function and the bulk flow simultaneously do exist though, see, e.g., [4].)

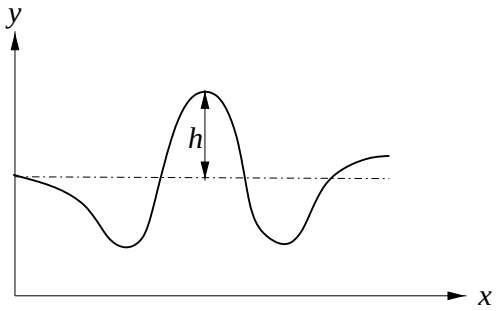

Figure 2: Free-surface height h.

The number of conditions to be imposed on the free surface is one more than on fixed boundaries, it is equal to the usual number for the bulk flow (two conditions for the 2D Navier-Stokes equations, e.g.) plus one extra for the height function. For free-surface-flow problems as occurring in ship hydrodynamics, the simplest free-surface conditions express that the mass transport through and the stresses at the free surface are zero. Imposing these conditions in a physically correct way is of paramount importance for a good resolution of the free surface and is not trivial. One subtlety in case of, e.g., steady free-surface water waves is that these are known to satisfy dispersion relations [5], which uniquely relate the lengths of the free-surface waves under the action of gravity to the Froude number. Ideally, in the discrete case, these relations should be satisfied. Another point of attention is the intersection of the free surface and a no-slip boundary, an example of this is the water line at a ship's hull. Here, the (minor) difficulty is that in the unsteady case the free-surface and the no-slip boundary conditions do not match.

Because during the free surface's motion the grid may strongly distort, discretization of the flow equations in the computational domain is more appropriate than in the physical domain. A consequence is that because of the more intricate equations (due to the metric terms), it is harder to build in physics at a low discretization level.

For steady, free-surface-flow problems, a common solution approach (when using the free-surface-height method) is the following two-step process:

1. Solve the steady bulk-flow equations (the full Navier-Stokes equations, e.g.) with the free surface frozen and with – consequently – one free-surface condition not imposed.

2. On the basis of the previously obtained bulk-flow solution, correct the free surface such that it (better) satisfies the free-surface condition not imposed in the first step. If not yet converged for both bulk flow and free-surface flow, return to step 1.

A pitfall in making this solution process efficient is to make both steps efficient, ignoring their interaction. This holds in particular for step 2; introducing large free-surface updates may hamper or even ruin the bulk-flow problem's convergence to a steady state. For that reason, the rule in steady free-surface flow computations is to carefully march the unsteady free-surface and bulk-flow equations to a steady state. However, because of the persistent unsteady free-surface-flow phenomena, this evolutionary approach is not efficient at all. In [6], still following the above two-step process, an efficient method is proposed for solving the steady free-surface flow (step 2) whilst keeping the induced perturbations in the bulk flow (step 1) small. The key lies in the implementation of the free-surface conditions: in [6], a so-called quasi-free-surface condition is proposed. For smooth, singly-connected free surfaces, this method appears to work perfectly well [7, 8]. However, when steepening the water waves, as expected, its performance deteriorates and finally breaks down. In case of unsteady free-surface flows, the technique of alternatingly updating the bulk flow and the free surface may be followed as well. However, it is expected that this subcycling approach is only first-order accurate in time, independent of the separate accuracies of the time integrators for bulk flow and free-surface flow. (Evidence for this, in the application area of fluid-structure interactions, is given in [9].)

Fixed-grid methods hold out the promise of resolving a much larger class of free-surface flows and – also – of not suffering from a time accuracy barrier in the unsteady case. In the next section, we consider some pros and cons of fixed-grid techniques.

1.2.3 Fixed-grid techniques In the Eulerian approach, since many years, some well-proven techniques exist for computing flows with free boundaries. A classical method is the Marker-and-Cell (MAC) method [10]. In it, one of the two fluids is seeded with massless particles that go with the flow. A grid cell without any particle is defined to be a cell fully filled with the other fluid (possibly void) and the free surface(s) may be defined as the set(s) of cell faces separating the cells with particles from the cells without, or – more accurately – as the tight contour(s) wrapped around the particles such that no cell without particles is closed in (Figure 3a). Flow bifurcations cause no difficulties to the MAC method. A deficiency though is that no clear distinction can be made between physical and numerical cavitation (Figure 3a: empty cell at the bottom of the fluid). To avoid this uncertainty, the rule is to seed the fluid with as many particles as possible. Doing so, particularly in 3D, the MAC method may become very expensive.

A more efficient fixed-grid method is the Volume-of-Fluid (VOF) method [11]. In it, per grid cell, in addition to the standard fluid-flow quantities such as velocity and pressure, a scalar quantity is introduced, which represents the fraction of that cell, that is filled with one of the two fluids: the VOF fraction (Figure 3b). The fraction is transported by means of the advection equation. The location of the free surface can be defined in a similar way as in the MAC method, viz. as the set of cell faces separating the cells with the VOF fraction larger than zero from the cells with the VOF fraction equal to zero, or – more accurately – at the subcell level. The latter requires intricate flux algorithms, particularly in 3D. A principal drawback of the VOF method is that the VOF fraction is non-smooth and – hence – hard to accurately resolve in precisely the region of interest: at the free surface.

A natural fix is to replace the VOF fraction by a smooth scalar function, which represents, e.g., the distance to the free surface. Doing so, the free surface is simply defined as the zero-distance iso-surface. This is known as a level-set method (Figure 3c). A text book on level-set methods is [12], a classical journal paper is [13]. Older work in which the technique is already found, though not yet under the name of level-set technique, is that by Markstein on flame propagation. See, e.g., [14], in which a flame front is represented by a higher-dimensional, differentiable function that is advected by the flow. Since last decade, level-set methods enjoy many publications, a list related to CFD only is [15]–[30]. When computing the flow of a single fluid with free surface, i.e., a material-void interface, a minor problem of level-set methods is that no velocity field is defined in the void region. Hence, to guarantee smoothness of the level-set function, a proper artificial velocity field in the void region needs to be defined. This difficulty may also be seen as a good opportunity though to improve the free boundary's resolution without being inhibited by physics. E.g., in the void region an artificial velocity might be chosen which counteracts the effects of numerical diffusion by anti-advection [23, 31].

Keeping the level-set function smooth forms a point of attention. During the computation, the function may need to be regularized. In this reinitialization step, care needs to be taken that the free-surface location is preserved.

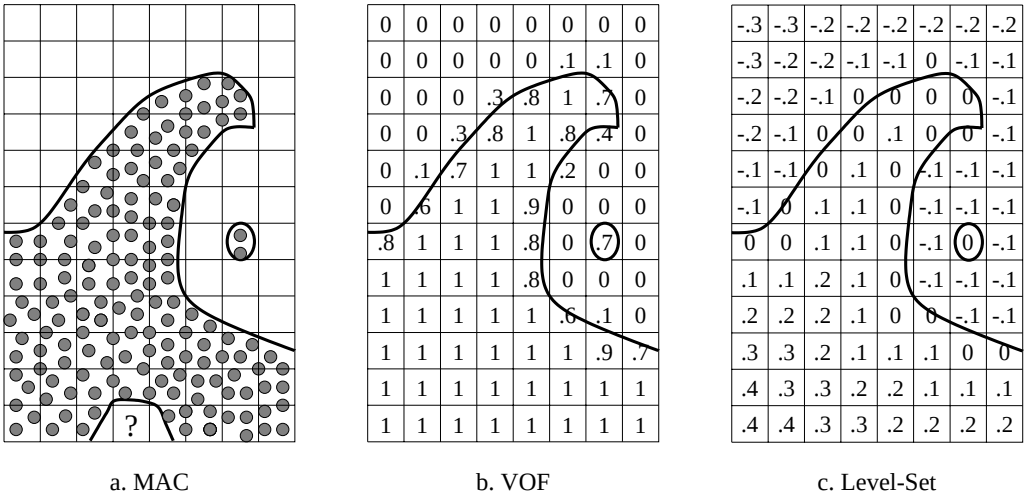

a. MAC b. VOF c. Level-Set

Figure 3: Known types of fixed-grid techniques for computing free-surface flows.

Using an MAC, a VOF or a level-set method, free-surface boundary conditions can be imposed at all cell faces separating the two fluids or – alternatively – at the subcell level. With a level-set method, the latter can be done more accurately than with the VOF method, but is still intricate, particularly in 3D. In [32], the approach of imposing free-surface conditions in the interior of the computational domain is called tracking. In some sense, imposing conditions on a free surface is a contradiction in terms. The free surface is genuinely free when it is *captured* (i.e., when no conditions at all are imposed on it). In capturing methods, in principle, the free surface is a two-fluid interface (with one fluid possibly virtual). The challenge of capturing methods is to choose or devise a physically correct two-fluid flux formula to be applied at the low discrete level of cell faces. A specific, well-known problem of capturing (not of tracking and fitting) techniques is that large solution errors may occur near the interface (the so-called 'pressure-oscillation problem'). In literature, several remedies against this have already been proposed. In a forthcoming paper we will also address this problem.

As mentioned, both tracking and capturing can be combined with the MAC, the VOF as well as the level-set method. In the present paper, we consider the combination of a capturing scheme and a level-set technique. A novel capturing scheme suitable for two-fluid flows, in particular liquid-gas (water-air) problems, is proposed. As compared to the surface-height method, with the MAC, VOF and level-set

methods, computational overhead has been introduced by the representation of the n-dimensional free surface as an $(n+1)$-dimensional set of particles (MAC) or function (VOF and level-set). When computing a single-fluid-flow problem with free surface by a capturing technique, even more overhead is introduced by the computation of the flow of the virtual second fluid. The overhead is expected to be counterbalanced to an amply sufficient degree by the advantages of capturing: no remeshing, no limitation with respect to free-surface topologies, no free-surface boundary conditions to be imposed (the dispersion relations in case of water waves under the action of gravity, e.g., will be satisfied automatically), etc.

1.3 Point of departure

The present work is directed towards two-fluid-flow computations on the basis of the Navier-Stokes equations, excluding phenomena such as surface tension, mixing of the fluids, and condensation and vaporization. Diffusion and gravity are still planned for future work, here the homogeneous Euler equations are considered.

In [32], Kelecy & Pletcher consider capturing for incompressible two-fluid-flow equations, which are balanced through the zero-divergence relation for the velocity field. In a capturing technique for the flow of two fluids with different densities, density is an unknown even in the incompressible case. Given this fact, a compressible approach will not necessarily be much more computing-intensive. The foreseen applications are homentropic, yielding – for perfect gases and liquids – equations of state of the compact form $p = p(\rho)$. Hence, to balance the equations, no energy equation needs to be invoked. Use of the compressible fluid-flow equations has the following advantages over the incompressible:

- The unpleasant property of weak coupling between continuity equation and momentum equations (through velocity only) is avoided. Advantage can be taken of numerical techniques with built-in physics, which have been developed already for gas-dynamics applications. E.g., at each cell face, a local 1D Riemann problem can be considered (Godunov approach). With this, it should be possible to resolve in a physically correct way the two-fluid interface (represented by the contact discontinuity) over a single cell face or cell only. In such a compressible approach, there will be no need for, e.g., staggering or – in case of unsteady flow simulation – pseudo-time stepping.

- In principle, the compressible approach is always more correct. For very low-Mach number flows, it may still be preferable when, e.g., large characteristic lengths play a role. The time needed by pressure disturbances to travel along a ship's hull, e.g., may be significant. (Denoting the characteristic length and time by l and τ, respectively, and the flow speed and speed of sound by u and c, with the for ship hydrodynamics realistic values $l = 100$ m, $u + c \approx c \approx 1000$ m/sec, it follows $\tau = l/(u+c) = 0.1$ sec, which may not be negligible in unsteady flow simulations.) In low-Mach-number hydraulics problems such as the simulation of the impact of storm surges on dikes, compressibility is even mandatory. (Air enclosed by water wave and dike will behave as an airbag; compressibility is essential in the dynamics of these flow problems.) For the known difficulties of low-Mach number flows (poor solvability and reduced accuracy) many fixes have been proposed, see, e.g., [33]–[41], and [42], p. 578 for more recent work.

1.4 Outline of paper

In the present paper, the emphasis still lies on the development of a liquid-gas Godunov-type scheme, in combination with a level-set technique, i.e., on flows with a single spatial dimension only.

The contents of the paper is the following. In Section 2, the continuous flow model is given (conservation laws, equation of state and level-set equation). In Section 3, the space discretization of the equations is presented (the Riemann problem and corresponding Godunov-type scheme, at both interior and boundary cell faces). In Appendix A, we show that this scheme is a linearized, two-fluid Godunov scheme.

2. Flow model

2.1 Conservation equations

The two fluids do not mix. Denoting the densities of the two fluids by ρ_1 and ρ_2, this implies that if $\rho_1 > 0$ then $\rho_2 = 0$ and – vice versa – if $\rho_2 > 0$ then $\rho_1 = 0$. (See Figure 4 for a 1D illustration with x_{fs} the location of the free surface.)

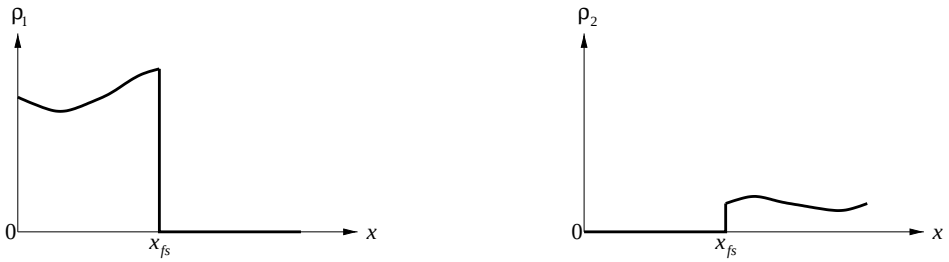

a. Fluid 1 b. Fluid 2

Figure 4: Density distributions in 1D flow of two immiscible fluids.

The immiscibility also implies that $u_1(x_{fs}) = u_2(x_{fs}) = u(x_{fs})$; the free surface is a contact discontinuity. The separate masses of the two fluids need to be conserved. In 1D, this means for a control volume Ω:

$$\int_\Omega \frac{d\rho_1}{dt} dx + (\rho_1 u)_{\partial\Omega_{right}} - (\rho_1 u)_{\partial\Omega_{left}} = 0, \tag{2.1a}$$

$$\int_\Omega \frac{d\rho_2}{dt} dx + (\rho_2 u)_{\partial\Omega_{right}} - (\rho_2 u)_{\partial\Omega_{left}} = 0. \tag{2.1b}$$

For the control volume Ω we may next define the bulk density $\rho \equiv \frac{\int_\Omega (\rho_1+\rho_2) dx}{\int_\Omega dx}$, which for sufficiently small Ω can be approximated by $\rho = \frac{\rho_1 V_1 + \rho_2 V_2}{V_1+V_2}$, where V_1 and V_2 are the sizes of the subvolumes of Ω that are filled with fluid 1 and fluid 2, respectively. (So, it has been assumed that ρ_1 and ρ_2 are constant over V_1 and V_2, respectively.) Introducing the volume fraction α of fluid 1, $\alpha = \frac{V_1}{V_1+V_2}$, we can write

$$\rho = \alpha\rho_1 + (1-\alpha)\rho_2, \quad \alpha \in [0,1]. \tag{2.2}$$

An alternative for (2.1) is then

$$\int_\Omega \frac{d\rho}{dt} dx + (\rho u)_{\partial\Omega_{right}} - (\rho u)_{\partial\Omega_{left}} = 0, \tag{2.3}$$

plus a still to be filled in equation for the location(s) x_{fs} of the interface(s) in space and time. The latter equation determines $\alpha = \alpha(x,t)$. Looking ahead at the differences between both formulations in a numerical implementation, we already note that with the bulk-density formulation, in a finite-volume discretization, total mass of the fluid will be conserved, but not necessarily the masses of the two separate fluids. In case $\alpha(x,t)$ is not exactly resolved, the two separate masses are not conserved. As opposed to that, with formulation (2.1) in a finite-volume discretization, the masses of the separate fluids are always exactly conserved. Hence, when using formulation (2.3), an accurate resolution of the interface location(s) is of paramount importance.

As far as momentum is concerned, the bulk density is a more practical quantity than the densities of the two separate fluids, because – as opposed to mass – the momenta of the two fluids do not need

to be conserved separately. Only the total amount does, the two fluids can exchange momentum. Because surface tension is not considered, it also holds $p_1(x_{fs}) = p_2(x_{fs}) = p(x_{fs})$. So, for the momentum equation we can write

$$\int_\Omega \frac{d(\rho u)}{dt} dx + (\rho u^2 + p)_{\partial\Omega_{right}} - (\rho u^2 + p)_{\partial\Omega_{left}} = 0. \tag{2.4}$$

To describe two-fluid flows, we opt for the bulk-density description, i.e., equations (2.2)–(2.4). The system of equations is not yet balanced. There are six unknowns: $\rho_1, \rho_2, \rho, p, u$ and α. The equation for the location of the interface (determining α) still has to be chosen. For this, we follow a level-set approach, to be discussed in the next section. For the remaining unknowns ρ_1 and ρ_2, equations of state $\rho_1(p)$ and $\rho_2(p)$ are chosen in Section 2.3.

2.2 level-set equation

As mentioned, to conserve the masses of the separate fluids as accurately as possible when using the bulk-density formulation, it is essential to resolve the free-surface locations as accurately as possible. For that purpose, the level-set approach is (in principle) better suited than the VOF approach, because of its better smoothness properties. Good smoothness of the level-set function is first taken care of in the level-set function's initialization. A common approach is to initialize the level-set function as the signed distance to the initial free surface, with the distance positive in – say – fluid 1 and negative in fluid 2. The choice for the signed-distance function may not be attractive though. In case of, e.g., a 1D flow problem with two interfaces (Figure 5), the level-set function defined as the signed-distance

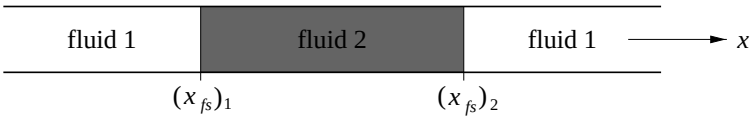

Figure 5: 1D two-fluid flow with two interfaces.

function would look as depicted in Figure 6a, i.e., perfectly smooth at both free surfaces, but with a non-differentiability in between. Denoting the level-set function by ϕ, in formula, the function in Figure 6a reads

$$\phi(x) = \min\left(x - (x_{fs})_1, (x_{fs})_2 - x\right). \tag{2.5a}$$

The level-set function does not need to be the signed-distance function. An alternative for it, which is uniformly smooth but non-zero at the free surface is sketched in Figure 6b. In formula, here, one may think of, e.g.,

$$\phi(x) = e^{-(x-(x_{fs})_1)^2(x-(x_{fs})_2)^2} - 1. \tag{2.5b}$$

In [23], numerical experiments are done with level-set functions similar to the latter. For our present applications, the level-set function does not need to be uniformly smooth, only at the interfaces it must be. It is preferred to be linear there. Therefore, in the present paper we do take the signed-distance function as the initial level-set function.

The level-set function is advected by, in 1D:

$$\frac{\partial \phi}{\partial t} + u\frac{\partial \phi}{\partial x} = 0, \tag{2.6}$$

with u the local velocity. Combined with bulk-mass conservation equation (2.3), quasi-linear equation (2.6) may be written in the conservative control-volume form

$$\int_\Omega \frac{d(\rho \phi)}{dt} dx + (\rho u \phi)_{\partial\Omega_{right}} - (\rho u \phi)_{\partial\Omega_{left}} = 0. \tag{2.7}$$

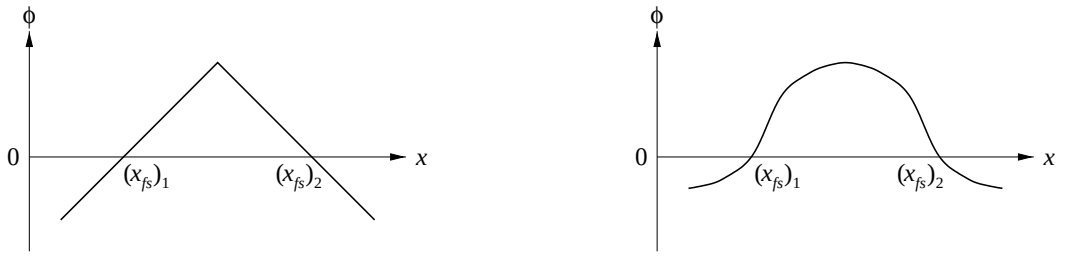

a. Signed-distance function b. Continuously differentiable function

Figure 6: Possible initial level-set functions for 1D two-fluid flow with two interfaces.

Conservation of $\rho\phi$ is not important, there is no conservation law for it. The form (2.7) is simply practical because it is consistent with the system (2.3)–(2.4), it can be directly added to it. As soon as the level-set function becomes insufficiently smooth during its advection (assuming there is a smoothness criterion available), it must be regularized. Crucial in this reinitialization is that the free-surface location(s) at that specific moment are preserved as accurately as possible. (If this is not taken care of, the reinitialization can be even counterproductive.)

The advantages of level-set methods over particularly VOF methods are:

- Level-set functions are smooth at physical discontinuities and – hence – can be advected in a numerically accurate way precisely there. As opposed to that, the less smooth VOF function may easily smear out or become non-monotonous during its advection, thus deteriorating the resolution of the free surface.
- The level-set equation can be directly embedded into the system of fluid-flow equations and discretized collectively and consistently with these. E.g., it can be included into the Godunov-type scheme, which is what we will do. Related to this, there is no principal difficulty in extending a 1D level-set technique to multi-D.

2.3 Equations of state

In our water-air computations, for both fluids, elegant use can be made of a single equation of state, Tait's [43, 44]:

$$\frac{p + Bp_\infty}{(1+B)p_\infty} = \left(\frac{\rho}{\rho_\infty}\right)^\gamma, \tag{2.8}$$

where the subscript ∞ refers to some reference state. For water, it holds (at sea level conditions): $\gamma = 7$, $B = 3000$, $\rho_\infty = 1000$ kg/m^3, and for air: $\gamma = \frac{7}{5}$, $B = 0$, $\rho_\infty = 1$ kg/m^3. With (2.8), both the water and air density, to be denoted from now on by $\rho_w(p)$ and $\rho_a(p)$, are convex functions of pressure. Likewise, the corresponding bulk density

$$\rho(\phi, p) = \alpha(\phi)\rho_w(p) + (1 - \alpha(\phi))\rho_a(p), \quad \alpha(\phi) \in [0,1] \tag{2.9}$$

is. The physical consequences of this overall convexity are that neither locally very low speeds of sound (much lower than in pure water or pure air), nor entropy-condition-satisfying expansion shocks can occur. These two anomalous phenomena are typical for flows with mixed convex-concave equations of state, flows with, e.g., condensation or vaporization [45], and cannot occur in the immiscible two-fluid flows considered here. To give some more evidence of this, consider the speed of sound of the bulk fluid: $c^2 = \frac{\partial p}{\partial \rho}$. Using (2.9), we can write $\frac{1}{c^2} = \frac{\alpha}{c_w^2} + \frac{1-\alpha}{c_a^2}$, with $c_w^2 = \left(\frac{d\rho_w}{dp}\right)^{-1}$ and $c_a^2 = \left(\frac{d\rho_a}{dp}\right)^{-1}$. So,

$$c^2 = \frac{c_w^2 c_a^2}{\alpha c_a^2 + (1-\alpha)c_w^2}. \tag{2.10}$$

Assuming that for any given p, $c_a < c_w$, from (2.10) it is seen that $c_a \leq c \leq c_w$ for all $\alpha \in [0,1]$. For clarity, we also give a graphical illustration. In two-phase flows with condensation or vaporization, the pressure-density diagram may look as sketched in Figure 7a, i.e., as a mixed convex-concave curve with extremely small values of the speed of sound, $\frac{dp}{d\rho}$, in the condensation/vaporization zone. As opposed to that, in the case of two immiscible fluids, a family of purely convex curves exists, curves that become increasingly steeper for increasing α (Figure 7b). So, for any p and for all values of $\alpha \in (0,1)$ it holds $c_a < c < c_w$.

A slight inconvenience of the nonlinear equation of state (2.8) in combination with (2.9) is that the calculation of p for known ρ and α ($\alpha \neq 0$ and $\alpha \neq 1$) needs to be done iteratively.

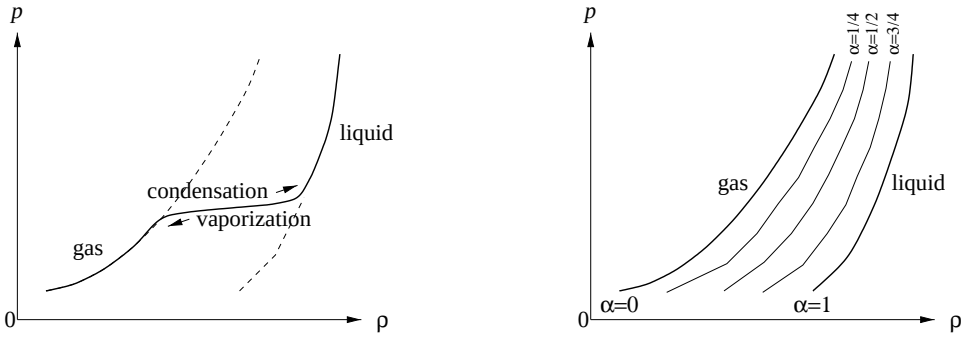

a. For two-phase flows b. For immiscible two-fluid flows

Figure 7: Pressure-density diagrams.

3. Discretization

3.1 Finite volumes

Summarizing, for a (sufficiently small) control volume Ω, the system of equations considered reads

$$\int_\Omega \frac{dq}{dt}dx + (f(q))_{\partial\Omega_{right}} - (f(q))_{\partial\Omega_{left}} = 0, \quad q = \begin{pmatrix} \rho \\ \rho u \\ \rho\phi \end{pmatrix}, \quad f(q) = \begin{pmatrix} \rho u \\ \rho u^2 + p \\ \rho u\phi \end{pmatrix}, \tag{3.1a}$$

$$\rho = \alpha(\phi)\rho_w(p) + (1-\alpha(\phi))\rho_a(p),$$
$$\rho_w(p) = \left(\frac{p + B_w p_\infty}{(1+B_w)p_\infty}\right)^{\frac{1}{\gamma_w}} (\rho_w)_\infty, \quad \rho_a(p) = \left(\frac{p + B_a p_\infty}{(1+B_a)p_\infty}\right)^{\frac{1}{\gamma_a}} (\rho_a)_\infty, \tag{3.1b}$$
and with $\alpha(\phi)$ the fraction of the size of Ω over which $\phi \geq 0$.

The natural discretization for (3.1a) is a finite-volume technique. We consider cell-centered finite volumes with, for simplicity, constant mesh size h. This choice directly allows us to work out the discretization of $\alpha(\phi)$. Consider finite volume Ω_i and its left and right neighbors (Figure 8) and define the level-set values at the cell faces $\partial\Omega_{i-\frac{1}{2}}$ and $\partial\Omega_{i+\frac{1}{2}}$ as

$$\phi_{i-\frac{1}{2}} = \frac{1}{2}(\phi_{i-1} + \phi_i), \quad \phi_{i+\frac{1}{2}} = \frac{1}{2}(\phi_i + \phi_{i+1}). \tag{3.2}$$

Then, for $\phi_i \geq 0$, we propose the following expression for α_i:

$$\phi_{i-\frac{1}{2}} \geq 0,\ \phi_{i+\frac{1}{2}} \geq 0: \quad \alpha_i = 1, \tag{3.3a}$$

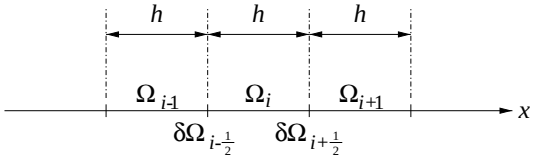

Figure 8: Finite volume Ω_i and its two neighbors.

$$\phi_{i-\frac{1}{2}} < 0,\ \phi_{i+\frac{1}{2}} \geq 0: \quad \alpha_i = \frac{1}{2}\left(\frac{\phi_i}{\phi_i - \phi_{i-\frac{1}{2}}} + 1\right), \tag{3.3b}$$

$$\phi_{i-\frac{1}{2}} \geq 0,\ \phi_{i+\frac{1}{2}} < 0: \quad \alpha_i = \frac{1}{2}\left(1 + \frac{\phi_i}{\phi_i - \phi_{i+\frac{1}{2}}}\right), \tag{3.3c}$$

$$\phi_{i-\frac{1}{2}} < 0,\ \phi_{i+\frac{1}{2}} < 0: \quad \alpha_i = \frac{1}{2}\left(\frac{\phi_i}{\phi_i - \phi_{i-\frac{1}{2}}} + \frac{\phi_i}{\phi_i - \phi_{i+\frac{1}{2}}}\right). \tag{3.3d}$$

The four possibilities in (3.3) are illustrated in Figure 9. So, in determining $\phi_{i-\frac{1}{2}}$ and $\phi_{i+\frac{1}{2}}$, as well as $x(\phi = 0)$, use is made of piecewise linear interpolation of ϕ. The linear interpolation is exact as long as the level-set function is the signed-distance function. (As soon as this distance property is lost, the exact conservation of the separate water and air masses is lost.) For $\phi_i < 0$, similar expressions can be written. (Using this similarity, the system of expressions for α_i can be coded compactly.)

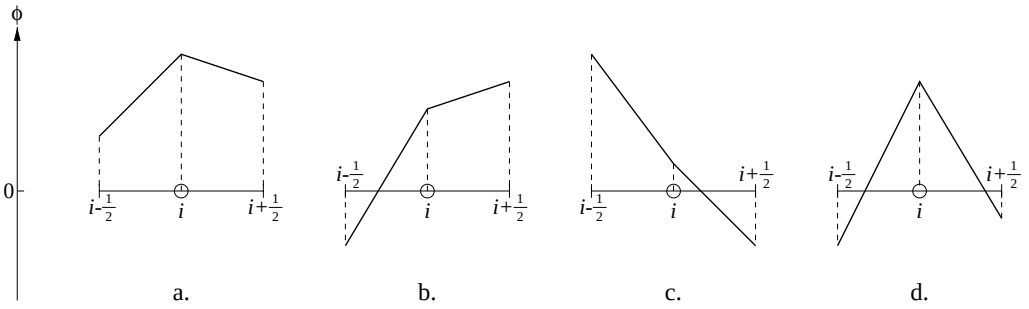

Figure 9: Four possible combinations of signs of $\phi_{i-\frac{1}{2}}$ and $\phi_{i+\frac{1}{2}}$, $\phi_i \geq 0$.

3.2 Riemann-problem approach

For the control-volume formulation, we need a formula for the flux vector across a cell face. The formula must have built-in physics for accurately capturing the free surface. For that purpose, trivial, term-by-term flux formulae such as, e.g., $(f(q))_{i+\frac{1}{2}} = f\left(\frac{1}{2}(q_i + q_{i+1})\right)$ are less appropriate than formulae derived from the Riemann problem. Besides a good capturing of the free surface, a Riemann problem approach is expected to yield robustness and a good boundary-condition treatment. For ship hydrodynamics applications, a physically proper discretization of convection terms may be as relevant as for aircraft and spacecraft aerodynamics. The convection phenomena in ship hydrodynamics are less rich (no supersonic speeds), but the Reynolds numbers are generally higher (up to $\mathcal{O}(10^9)$). The exact solution of the 1D Riemann problem on each cell face, Godunov's approach [46], requires the exact computation of the cell-face state. For the current equations, this implies the use of a numerical

root finder. We avoid this by considering an approximate Riemann solver: Osher's [47], to start with. Denoting the left and right cell-face state by q_0 and q_1, and the flux formula by $F(q_0, q_1)$, Osher's approximate Riemann solver may be written as

$$F(q_0, q_1) = f(q_0) + \int_{q_0}^{q_1} \frac{df^-}{dq} dq, \tag{3.4}$$

with $\frac{df^-}{dq}$ the negative eigenvalue part of the Jacobian $\frac{df}{dq}$. The eigenvalues of the present Jacobian are: $\lambda_1 = u - \sqrt{\frac{\partial p}{\partial \rho}}$, $\lambda_2 = u$, $\lambda_3 = u + \sqrt{\frac{\partial p}{\partial \rho}}$. ($\frac{\partial p}{\partial \phi}$ does not occur in the wave speeds.) For the right eigenvectors we refer to [48], presented there for the 3D situation. The Riemann-invariant relations describing the two intermediate states $q_{\frac{1}{3}}$ and $q_{\frac{2}{3}}$ along the wave path in state space (Figure 10) are

$$u_{\frac{1}{3}} + \int^{\rho_{\frac{1}{3}}} \frac{1}{\rho} \sqrt{\frac{\partial p}{\partial \rho}} d\rho = u_0 + \int^{\rho_0} \frac{1}{\rho} \sqrt{\frac{\partial p}{\partial \rho}} d\rho, \tag{3.5a}$$

$$\phi_{\frac{1}{3}} = \phi_0, \tag{3.5b}$$

$$u_{\frac{1}{3}} = u_{\frac{2}{3}} = u_{\frac{1}{2}}, \tag{3.6a}$$

$$p_{\frac{1}{3}} = p_{\frac{2}{3}} = p_{\frac{1}{2}}, \tag{3.6b}$$

$$u_{\frac{2}{3}} - \int^{\rho_{\frac{2}{3}}} \frac{1}{\rho} \sqrt{\frac{\partial p}{\partial \rho}} d\rho = u_1 - \int^{\rho_1} \frac{1}{\rho} \sqrt{\frac{\partial p}{\partial \rho}} d\rho, \tag{3.7a}$$

$$\phi_{\frac{2}{3}} = \phi_1. \tag{3.7b}$$

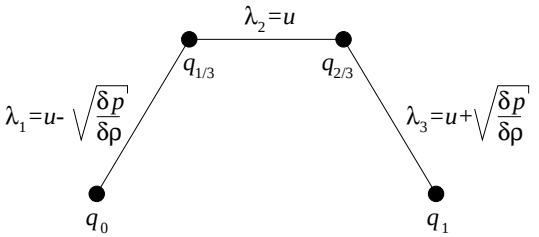

Figure 10: Wave path in state space for immiscible two-fluid flow.

The level-set function ϕ can change along the subpath corresponding with the eigenvalue λ_2, i.e., as it should be, across the contact discontinuity. It is invariant along the outer subpaths, i.e., along both subpaths the distance to the free surface is constant. Through the known Riemann invariants u and p at the contact discontinuity, the kinematic and dynamic free-surface boundary conditions (zero mass transport and stresses) are satisfied. The integrals in (3.5a) and (3.7a) can be written out explicitly for the equations given in (3.1b). However, when a free surface is captured, i.e., when $\phi_{\frac{1}{3}}$ and $\phi_{\frac{2}{3}}$ differ in sign, explicit calculation of $u_{\frac{1}{2}}$ and $p_{\frac{1}{2}}$ is hampered by nonlinearity, the aforementioned drawback of Osher's scheme. (A transcendental equation needs to be solved.) Of course, $u_{\frac{1}{2}}$ and $p_{\frac{1}{2}}$ can then be determined numerically. Given foreseen future applications in which $u_{\frac{1}{2}}$ and $p_{\frac{1}{2}}$ need to be differentiated with respect to q_0 and q_1, we do not do so and propose another approximate Riemann solver in the next section.

3.3 Two-fluid, linearized Godunov scheme

Since ϕ is constant along the two outer subpaths of the wave path in Figure 10, along both subpaths the bulk density can only vary due to pressure changes. Because the flows to be considered are uniformly low-subsonic, large density changes will not occur there and – consequently – the integrals $\int^{\rho_{\frac{1}{3}}} \frac{1}{\rho}\sqrt{\frac{\partial p}{\partial \rho}}d\rho$ and $\int^{\rho_{\frac{2}{3}}} \frac{1}{\rho}\sqrt{\frac{\partial p}{\partial \rho}}d\rho$ can be linearized by good approximation around ρ_0 and ρ_1, respectively. Linearization of (3.5a) and (3.7a) yields

$$u_{\frac{1}{2}} = u_0 - (\rho_{\frac{1}{3}} - \rho_0)\frac{c_0}{\rho_0}, \tag{3.8a}$$

$$u_{\frac{1}{2}} = u_1 + (\rho_{\frac{2}{3}} - \rho_1)\frac{c_1}{\rho_1}. \tag{3.8b}$$

Likewise, $p_{\frac{1}{2}}$ can be linearized around ρ_0 and ρ_1:

$$p_{\frac{1}{2}} = p_0 + (\rho_{\frac{1}{3}} - \rho_0)c_0^2, \tag{3.9a}$$

$$p_{\frac{1}{2}} = p_1 + (\rho_{\frac{2}{3}} - \rho_1)c_1^2. \tag{3.9b}$$

Elimination of $\rho_{\frac{1}{3}} - \rho_0$ and $\rho_{\frac{2}{3}} - \rho_1$ from (3.8) and (3.9) yields

$$\frac{p_{\frac{1}{2}} - p_0}{u_{\frac{1}{2}} - u_0} = -C_0, \quad C_0 \equiv \rho_0 c_0, \tag{3.10a}$$

$$\frac{p_{\frac{1}{2}} - p_1}{u_{\frac{1}{2}} - u_1} = C_1, \quad C_1 \equiv \rho_1 c_1, \tag{3.10b}$$

i.e.,

$$\begin{pmatrix} u_{\frac{1}{2}} \\ p_{\frac{1}{2}} \end{pmatrix} = \begin{pmatrix} \frac{C_0 u_0 + C_1 u_1 + (p_0 - p_1)}{C_0 + C_1} \\ \frac{C_1 p_0 + C_0 p_1 + C_0 C_1 (u_0 - u_1)}{C_0 + C_1} \end{pmatrix}, \tag{3.11a}$$

with for the density and level-set function in the two intermediate points:

$$\begin{pmatrix} \rho_{\frac{1}{3}} \\ \phi_{\frac{1}{3}} \end{pmatrix} = \begin{pmatrix} \rho_0 + \frac{p_{\frac{1}{2}} - p_0}{c_0^2} \\ \phi_0 \end{pmatrix}, \tag{3.11b}$$

$$\begin{pmatrix} \rho_{\frac{2}{3}} \\ \phi_{\frac{2}{3}} \end{pmatrix} = \begin{pmatrix} \rho_1 + \frac{p_{\frac{1}{2}} - p_1}{c_1^2} \\ \phi_1 \end{pmatrix}. \tag{3.11c}$$

Excluding all supersonic possibilities from the matrix in Figure 11, which shows all possible combinations of eigenvalue signs along the wave path, (note the consequent improvement in efficiency!) the two-fluid, linearized Osher scheme reads then:

$$F(q_0, q_1) = f(q_{\frac{1}{3}}) = \begin{pmatrix} \rho_{\frac{1}{3}} u_{\frac{1}{2}} \\ \rho_{\frac{1}{3}} u_{\frac{1}{2}}^2 + p_{\frac{1}{2}} \\ \rho_{\frac{1}{3}} u_{\frac{1}{2}} \phi_{\frac{1}{3}} \end{pmatrix}, \quad \text{if } u_{\frac{1}{2}} \geq 0, \tag{3.12a}$$

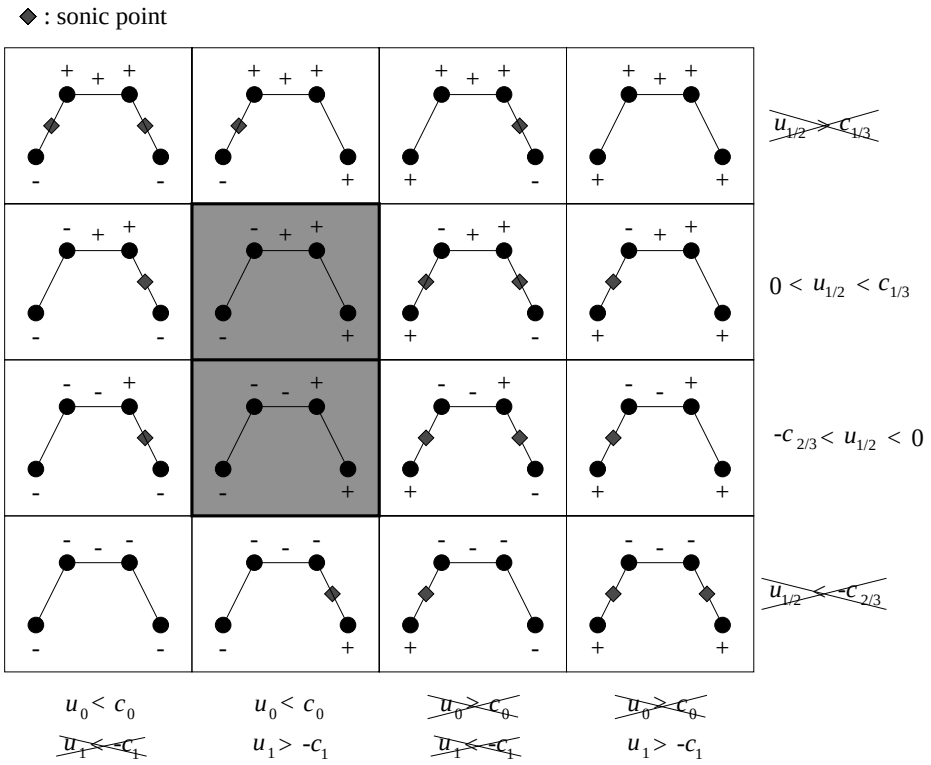

Figure 11: All possible eigenvalue-sign combinations along wave path from Figure 10, crossed out: all supersonic speeds.

$$F(q_0, q_1) = f(q_{\frac{2}{3}}) = \begin{pmatrix} \rho_{\frac{2}{3}} u_{\frac{1}{2}} \\ \rho_{\frac{2}{3}} u_{\frac{1}{2}}^2 + p_{\frac{1}{2}} \\ \rho_{\frac{2}{3}} u_{\frac{1}{2}} \phi_{\frac{2}{3}} \end{pmatrix}, \quad \text{if } u_{\frac{1}{2}} \leq 0. \tag{3.12b}$$

Note that the real nonlinear flux functions $f(q_{\frac{1}{3}})$ and $f(q_{\frac{2}{3}})$ are applied, and not $F(q_0, q_1) = f(q_0) + (q_{\frac{1}{3}} - q_0)\frac{df(q_0)}{dq}$ if $u_{\frac{1}{2}} \geq 0$ and $F(q_0, q_1) = f(q_1) + (q_{\frac{2}{3}} - q_1)\frac{df(q_1)}{dq}$ if $u_{\frac{1}{2}} \leq 0$. There is no need for the latter linearized formulae. On the contrary, as opposed to (3.11)–(3.12), they may give rise to an erroneous, ambiguous flux at $u_{\frac{1}{2}} = 0$ (steady free surface); $f(q_0) + (q_{\frac{1}{3}} - q_0)\frac{df(q_0)}{dq}$ and $f(q_1) + (q_{\frac{2}{3}} - q_1)\frac{df(q_1)}{dq}$ may be different for $u_{\frac{1}{2}} = 0$.

For the single-fluid case, (3.12) reduces to

$$F(q_0, q_1) = \begin{pmatrix} \rho_{\frac{1}{2}} u_{\frac{1}{2}} \\ \rho_{\frac{1}{2}} u_{\frac{1}{2}}^2 + p_{\frac{1}{2}} \end{pmatrix}, \quad \rho_{\frac{1}{2}} = \rho(p_{\frac{1}{2}}), \tag{3.13}$$

with $u_{\frac{1}{2}}$ and $p_{\frac{1}{2}}$ still given by (3.11a). The latter scheme is known, see Section 2.3 and Appendix A in [49], and also Section 9.3 in [50]. It is the single-fluid, linearized Godunov scheme. In Appendix A of the present paper, through a (partial) derivation of the (exact) Godunov scheme, it is shown that the present two-fluid, linearized Osher scheme (3.10)–(3.11) is in fact the two-fluid, linearized Godunov scheme. For clarity, in the following, we only use the latter name for scheme (3.11)–(3.12).

3.4 Boundary-condition treatment
The boundary of the computational domain is formed by cell faces. The fluxes across the boundary faces can be computed with (3.12) as well. Denoting the state at the boundary by q_b, in case of a left boundary $q_0 = q_b$ and in case of a right $q_1 = q_b$. For (subsonic) inflow, in 1D, two of the three components of q_b must be imposed, reducing the wave path of the two-fluid, linearized Godunov scheme (Figure 12). In case of (subsonic) outflow, a single component of q_b must be imposed, leading to the reduced paths given in Figure 13.

a. Left boundary b. Right boundary

Figure 12: Reduced wave paths for inflow boundary.

a. Left boundary b. Right boundary

Figure 13: Reduced wave paths for outflow boundary.

With (3.4), for left inflow and left outflow it holds, as it should be, $F(q_b, q_1) = f(q_b)$ and for both right cases, correctly as well, $F(q_0, q_b) = f(q_0) + f(q_b) - f(q_0) = f(q_b)$. We work out the inflow and outflow boundary, and the non-permeable boundary as the limit case. For all three it holds, for boundary at the left:

$$\frac{p_b - p_1}{u_b - u_1} = C_1, \tag{3.14a}$$

and at the right:

$$\frac{p_b - p_0}{u_b - u_0} = -C_0. \tag{3.14b}$$

3.4.1 Inflow boundary The two boundary conditions to be imposed here cannot be u_b and p_b simultaneously; when u_b is imposed, p_b follows from (3.14). Vice versa, when p_b is imposed, u_b follows from (3.14). Hence, the second boundary condition must be one for ϕ_b. To compute the corresponding boundary flux $f(q_b) = \left(\rho_b u_b, \rho_b u_b^2 + p_b, \rho_b \phi_b\right)^T$, the '0D' bulk density still needs to be defined. (In 2D and 3D, the bulk density can be computed in a normal 1D and 2D way, respectively.) In 1D, an appropriate '0D' choice is

$$\rho_b = \rho_w(\phi_b), \quad \text{for } \phi_b \geq 0, \tag{3.15a}$$

$$\rho_b = \rho_a(\phi_b), \quad \text{for } \phi_b < 0. \tag{3.15b}$$

3.4.2 Outflow boundary Here, in addition to (3.14a) and (3.14b), the equations

$$\phi_b = \phi_0, \tag{3.16a}$$

$$\phi_b = \phi_1 \tag{3.16b}$$

are available. So, the single boundary condition to be imposed must be u_b, p_b, or some combination of both. The bulk density ρ_b is defined as in the inflow case.

3.4.3 Non-permeable boundary At a non-permeable boundary (at least) $u_b = 0$ must be imposed, which, given (3.14), already determines p_b. Considering a non-permeable boundary as the limit case of an inflow boundary, ϕ_b must still be imposed. Considering it as the limit of outflow, ϕ_b follows from the interior solution ($\phi_b = \phi_1$ for left boundary and $\phi_b = \phi_0$ for right). The latter limit case is to be preferred for, e.g., ship hydrodynamics applications. As opposed to in the first limit case, it allows the water line to freely move up and down the ship hull (Figure 14). Also here, the bulk density may be defined according to (3.15).

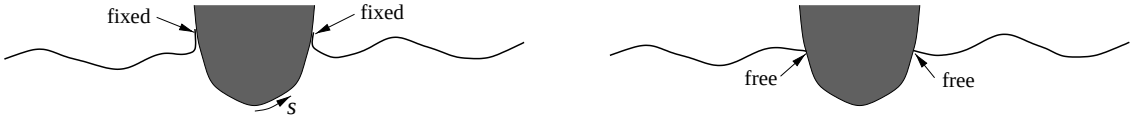

a. Fixed waterline, $\phi_b=\phi(s)$ a. Free waterline, $\phi_b=\phi_0$ or $\phi_b=\phi_1$

Figure 14: Cross section of ship hull with free surface.

4. Conclusions

To accurately compute compressible, immiscible two-fluid flows with very large density differences (water-air flows, e.g.) we have proposed a method that uses a level-set technique to distinguish between the two fluids. The resulting equations have been discretized through a finite-volume method. To compute the fluxes across the finite-volume walls (the level-set flux being one of the flux-vector components), we have proposed a two-fluid, linearized Godunov scheme. The scheme allows a physically correct capturing of the interface across a single cell face, as well as a neat boundary-condition treatment (no sticking of free surfaces to solid walls, e.g.). The scheme combines good physical properties with great simplicity and efficiency.

References

1. B.D. Nichols and C.W. Hirt, Calculating three-dimensional free surface flows in the vicinity of submerged and exposed structures, *J. Comput. Phys.*, **12**, 234–246 (1973).
2. J. Farmer, L. Martinelli and A. Jameson, A fast multigrid method for solving the nonlinear ship wave problem with a free surface, in Proceedings of the *Sixth International Conference on Numerical Ship Hydrodynamics*, Iowa (1993).
3. H.C. Raven, *A Solution Method for the Nonlinear Ship Wave Resistance Problem*, PhD-thesis, Delft University of Technology (1996).
4. B. Alessandrini and G. Delhommeau, A multigrid velocity-pressure free-surface-elevation fully coupled solver for calculation of turbulent incompressible flow around a hull, in Proceedings of the *21-st Symposium on Naval Hydrodynamics*, Trondheim (1996).
5. M.J. Lighthill, *Waves in Fluids*, Cambridge University Press, Cambridge (1978).
6. E.H. van Brummelen, Numerical solution of steady free-surface Navier-Stokes flow, *Report MAS-R0018*, CWI, Amsterdam (2000). http://www.cwi.nl/ftp/CWIreports/MAS/MAS-R0018.ps.Z.
7. E.H. van Brummelen, H.C. Raven and B. Koren, Numerical solution of steady free-surface Navier-Stokes flow, in Proceedings of the *First International Conference on Computational Fluid Dynamics*, Kyoto, 2000 (to appear).
8. E.H. van Brummelen, B. Koren and H.C. Raven, Efficient solution of steady free-surface Navier-Stokes flow, *Report MAS-R0103*, CWI, Amsterdam (2001). http://www.cwi.nl/ftp/CWIreports/MAS/MAS-R0103.ps.Z. (to appear in *J. Comput. Phys.*).
9. S. Piperno, C. Farhat and B. Larrouturou, Partitioned procedures for the transient solution of coupled aeroelastic problems. Part I: model problem, theory and two-dimensional application, *Comput. Methods Appl. Mech. Engrg.*, **124**, 79–112 (1995).
10. F.H. Harlow and J.E. Welch, Numerical calculation of time-dependent viscous incompressible flow of fluid with free surface, *Physics of Fluids*, **8**, 2182–2189 (1965).
11. C.W. Hirt and B.D. Nichols, Volume of fluid (VOF) method for the dynamics of free boundaries, *J. Comput. Phys.*, **39**, 201–225 (1981).
12. J.A. Sethian, *Level Set Methods: Evolving Interfaces in Geometry, Fluid Mechanics, Computer Vision, and Materials Science*, Cambridge University Press, Cambridge (1996).
13. W. Mulder, S. Osher and J.A. Sethian, Computing interface motion in compressible gas dynamics, *J. Comput. Phys.*, **100**, 209–228 (1992).
14. G.H. Markstein, Chapter B: Theory of flame propagation, in: *Non-Steady Flame Propagation* (G.H. Markstein, ed.), 5–14, Pergamon Press, New York (1964).
15. S.F. Davis, An interface tracking method for hyperbolic systems of conservation laws, *Appl. Numer. Math.*, **10**, 447–472 (1992).
16. J. Zhu and J.A. Sethian, Projection methods coupled to level set interface techniques, *J. Comput. Phys.*, **102**, 128–138 (1992).
17. M. Sussman, P. Smereka and S. Osher, A level set approach for computing solutions to incompressible two-phase flow, *J. Comput. Phys.*, **114**, 146–159 (1994).
18. H.-K. Zhao, T. Chan, B. Merriman and S. Osher, A variational level set approach to multiphase motion, *J. Comput. Phys.*, **127**, 179–195 (1996).
19. Y.C. Chang, T.Y. Hou, B. Merriman and S. Osher, A level set formulation of Eulerian interface capturing methods for incompressible fluid flows, *J. Comput. Phys.*, **124**, 449–464 (1996).

20. S. Chen, B. Merriman, S. Osher and P. Smereka, A simple level set method for solving Stefan problems, *J. Comput. Phys.*, **135**, 8–29 (1997).

21. J.-P. Cocchi and R. Saurel, A Riemann problem based method for the resolution of compressible multimaterial flows, *J. Comput. Phys.*, **137**, 265–298 (1997).

22. T.Y. Hou, Z. Li, S. Osher and H. Zhao, A hybrid method for moving interface problems with application to the Hele-Shaw flow, *J. Comput. Phys.*, **134**, 236–252 (1997).

23. B. Koren and A.C.J. Venis, A fed back level-set method for moving material-void interfaces, *J. Comput. Appl. Math.*, **101**, 131–152 (1999).

24. D. Adalsteinsson and J.A. Sethian, The fast construction of extension velocities in level set methods, *J. Comput. Phys.*, **148**, 2–22 (1999).

25. M. Sussman, A.S. Almgren, J.B. Bell, P. Colella, L.H. Howell and M.L. Welcome, An adaptive level set approach for incompressible two-phase flows, *J. Comput. Phys.*, **148**, 81–124 (1999).

26. B.T. Helenbrook, L. Martinelli and C.K. Law, A numerical method for solving incompressible flow problems with a surface of discontinuity, *J. Comput. Phys.*, **148**, 366–396 (1999).

27. R.P. Fedkiw, T. Aslam, B. Merriman and S. Osher, A non-oscillatory Eulerian approach to interfaces in multimaterial flows (the ghost fluid method), *J. Comput. Phys.*, **152**, 457–492 (1999).

28. M. Sussman and E.G. Puckett, A coupled level set and Volume-of-Fluid method for computing 3D and axisymmetric incompressible two-phase flows, *J. Comput. Phys.*, **162**, 301–337 (2000).

29. T.D. Aslam, A level-set algorithm for tracking discontinuities in hyperbolic conservation laws I. Scalar equations, *J. Comput. Phys.*, **167**, 413–438 (2001).

30. S.J. Osher and G. Tryggvason (eds.), Special issue on computational methods for multiphase flows, *J. Comput. Phys.*, **169 (2)** (2001).

31. C. Aalburg, *Experiments in Minimizing Numerical Diffusion across a Material Boundary*, MSc-thesis, Department of Aerospace Engineering, University of Michigan (1996). Also: http://www.engin.umich.edu/research/cfd/publications/publications.html

32. F.J. Kelecy and R.H. Pletcher, The development of a free surface capturing approach for multidimensional free surface flows in closed containers, *J. Comput. Phys.*, **138**, 939–980 (1997).

33. D. Choi and C.L. Merkle, Application of time-iterative schemes to incompressible flow, *AIAA J.*, **23**, 1518–1524 (1985).

34. E. Turkel, Preconditioned methods for solving the incompressible and low speed compressible equations, *J. Comput. Phys.*, **72**, 277–298 (1987).

35. B. van Leer, W.-T. Lee and P.L. Roe, Characteristic time-stepping or local preconditioning of the Euler equations, *AIAA Paper 91-1552* (1991).

36. G. Volpe, Performance of compressible codes at low Mach numbers, *AIAA J.*, **31**, 49–56 (1993).

37. Y.-H. Choi and C.L. Merkle, The application of preconditioning in viscous flows, *J. Comput. Phys.*, **105**, 207–223 (1993).

38. E. Turkel, Review of preconditioning methods for fluid dynamics, *Appl. Numer. Math.*, **12**, 257–284 (1993).

39. E. Turkel, A. Fiterman and B. van Leer, Preconditioning and the limit of the compressible to the incompressible flow equations for finite difference schemes, in *Computing the Future: Advances and Prospects for Computational Aerodynamics* (M.M. Hafez and D.A. Caughey, eds.), 215–234 Wiley, Chichester (1994).

40. B. Koren, Condition improvement for point relaxation in multigrid, subsonic Euler flow compu-

tations, *Appl. Numer. Math.*, **16**, 457–469 (1995).

41. B. Koren and B. van Leer, Analysis of preconditioning and multigrid for Euler flows with low-subsonic regions, *Advances in Comput. Math.*, **4**, 127–144 (1995).
42. P. Wesseling, *Principles of Computational Fluid Dynamics*, Springer, Berlin (2000).
43. P.G. Tait, *Voyage of H.M.S. Challenger*, 2(4), Stationery Office, London (1889).
44. G.K. Batchelor, *An Introduction to Fluid Dynamics*, Cambridge University Press, Cambridge (1967).
45. D.R. van den Heul, C. Vuik and P. Wesseling, A staggered scheme for hyperbolic conservation laws applied to unsteady sheet cavitation, *Computing and Vizualization in Science*, **2**, 63–68 (1999).
46. S.K. Godunov, Finite difference method for numerical computation of discontinuous solutions of the equations of fluid dynamics (Cornell Aeronautical Laboratory Translation from the Russian), *Math. Sbornik*, **47**, 271–306 (1959).
47. S. Osher and F. Solomon, Upwind difference schemes for hyperbolic systems of conservation laws, *Math. Comput.*, **38**, 339–374 (1982).
48. H. van Brummelen and B. Koren, A Godunov-type scheme for capturing water waves, in Proceedings of *Godunov Methods, Theory and Applications*, Oxford, 1999 (E.F. Toro, ed.), Kluwer, Dordrecht (to appear).
49. B. van Leer, Towards the ultimate conservative difference scheme, V. A second-order sequel to Godunov's method, *J. Comput. Phys.*, **32**, 101–136 (1979), also *J. Comput. Phys.*, **135**, 229–248 (1997).
50. E.F. Toro, *Riemann Solvers and Numerical Methods for Fluid Dynamics, A Practical Introduction*, Springer, Berlin (1997).
51. R. Courant and K.O. Friedrichs, *Supersonic Flow and Shock Waves*, Springer, Berlin (1976).

A. Two-fluid Godunov scheme for Tait's equation of state, derivation and linearization

A.1 State space, Poisson curves and Hugoniot curves

For the present two-fluid case, just as for the single-fluid case, in physical space, the left and right Riemann states (u_0, p_0) and (u_1, p_1) are connected to the intermediate state $(u_{\frac{1}{2}}, p_{\frac{1}{2}})$ through either a rarefaction wave or a shock wave. The four different possible pairs of shock and rarefaction waves that exist are sketched in Figure 15. In the single-fluid case, the four states $(u_{\frac{1}{2}}, p_{\frac{1}{2}})$ corresponding with

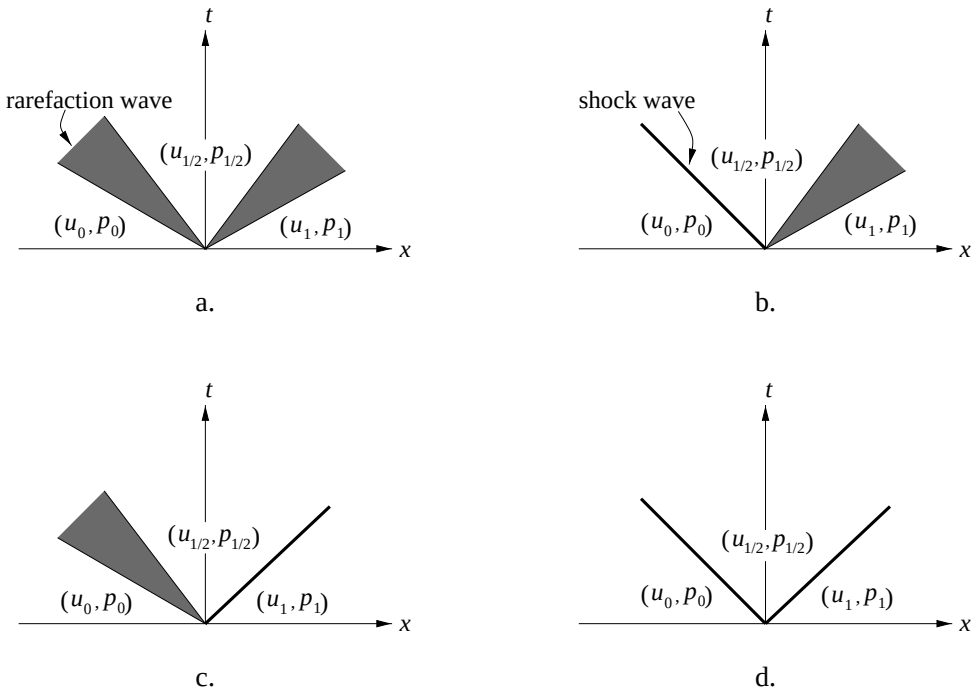

Figure 15: Wave combinations in physical space.

those in Figure 15 are determined as the intersection in the (u, p)-state space of either two Poisson curves (Figure 16a), a Poisson and a Hugoniot curve (Figures 16b and 16c), or two Hugoniot curves (Figure 16d). The Poisson curve through a point (u_k, p_k), $k = 0, 1$ represents all states (u, p) that can be reached from (u_k, p_k) through a rarefaction wave, the Hugoniot curve all points reachable through a shock wave. For details about this (single-fluid) theory, see [51], Sections 80 and 81. The specific forms of the Poisson and Hugoniot curves depend on the equation of state considered. In general, the curves are nonlinear. For a brief description of the two-fluid case on the basis of Tait's equation of state, see the next section.

A.2 Families of Poisson curves

For a two-fluid model in which the bulk density description (3.1b) is used, through a point (u_k, p_k), $k = 0, 1$ in state space, instead of a single Poisson curve, a family of Poisson curves exists, one curve for each value of the Volume-of-Fluid fraction α_k, $\alpha_k \in [0, 1]$, $k = 0, 1$. For rarefaction waves connecting (u_0, p_0) to $(u_{\frac{1}{2}}, p_{\frac{1}{2}})$, the family is determined by

$$u + \int^{p} \frac{1}{\rho c} dp = u_0 + \int^{p_0} \frac{1}{\rho c} dp, \tag{A.1a}$$

with the bulk density $\rho = \rho(\alpha_0, p)$ according to (3.1b) and the corresponding speed of sound $c = c(\alpha_0, p)$ according to (2.10), $\alpha_0 \in [0, 1]$. (Equation (A.1a) is equal to the first equation in (3.5a) with

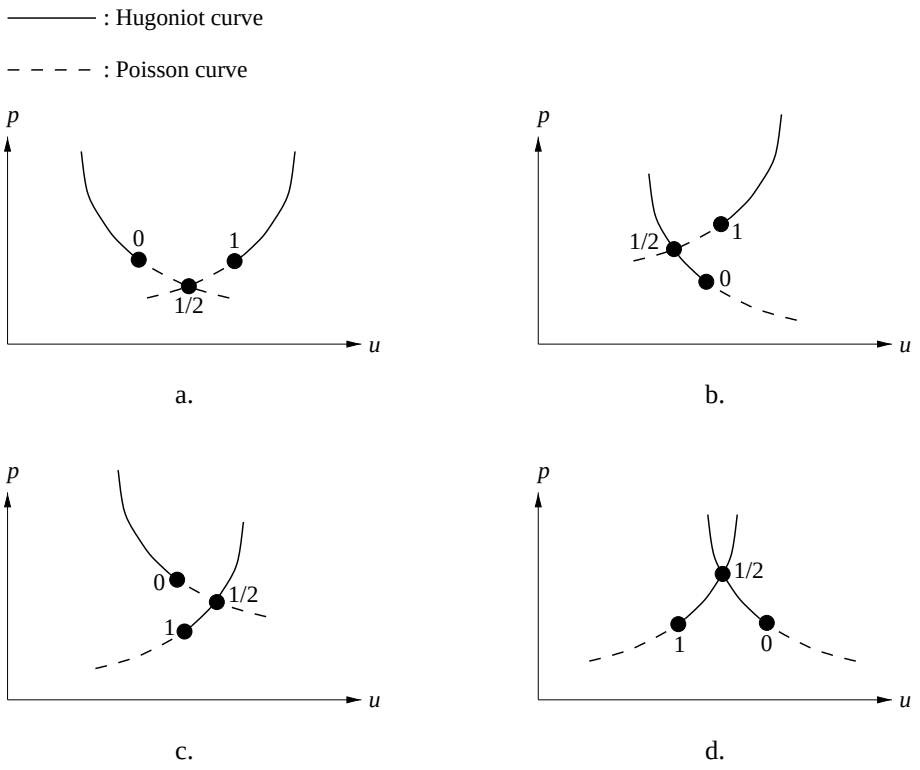

Figure 16: Poisson and Hugoniot curve combinations in state space, single-fluid, combinations a–d correspond with wave pairs in Figures 15a–d.

integration to p instead of to ρ.) For rarefactions connecting (u_1, p_1) to $(u_{\frac{1}{2}}, p_{\frac{1}{2}})$, the family of Poisson curves is determined by

$$u - \int^{p} \frac{1}{\rho c} dp = u_1 - \int^{p_1} \frac{1}{\rho c} dp, \tag{A.1b}$$

with the similar expressions for $\rho(\alpha_1, p)$ and $c(\alpha_1, p)$, $\alpha_1 \in [0,1]$. Finding formulae for the Poisson curves for general α_0 and α_1, $(\alpha_0, \alpha_1) \in \{[0,1] \times [0,1]\}$, is tedious. For convenience, here we consider the case $\alpha_0 = \alpha_1 = 1$ only (100% water in both the left and right control volume). For $\alpha = 1$, with Tait's equation of state, it holds

$$\rho(p) = \left(\frac{p + B_w p_\infty}{(1 + B_w) p_\infty} \right)^{\frac{1}{\gamma_w}} (\rho_\infty)_w, \tag{A.2a}$$

$$c(p) = \left(\frac{p + B_w p_\infty}{(1 + B_w) p_\infty} \right)^{\frac{\gamma_w - 1}{2\gamma_w}} (c_\infty)_w, \quad (c_\infty)_w = \sqrt{\gamma_w \frac{(1 + B_w) p_\infty}{(\rho_\infty)_w}}. \tag{A.2b}$$

Substitution of (A.2a) and (A.2b) into (A.1a) and (A.1b), and integration, yields for the exact Poisson curves

$$u - u_0 = \frac{-2}{\gamma_w - 1} \left[\left(\frac{p + B_w p_\infty}{(1 + B_w) p_\infty} \right)^{\frac{\gamma_w - 1}{2\gamma_w}} - \left(\frac{p_0 + B_w p_\infty}{(1 + B_w) p_\infty} \right)^{\frac{\gamma_w - 1}{2\gamma_w}} \right] (c_\infty)_w, \quad \text{for } \alpha_0 = 1, \tag{A.3a}$$

$$u - u_1 = \frac{2}{\gamma_w - 1}\left[\left(\frac{p + B_w p_\infty}{(1+B_w)p_\infty}\right)^{\frac{\gamma_w - 1}{2\gamma_w}} - \left(\frac{p_1 + B_w p_\infty}{(1+B_w)p_\infty}\right)^{\frac{\gamma_w - 1}{2\gamma_w}}\right](c_\infty)_w, \quad \text{for } \alpha_1 = 1. \tag{A.3b}$$

Linearization of (A.3a) and (A.3b) around (u_0, p_0) and (u_1, p_1), respectively, gives, denoting ρc by C:

$$\frac{p - p_0}{u - u_0} = \left(\frac{du}{dp}\right)^{-1}_{p_0} = -(C_0)_w, \quad \text{for } \alpha_0 = 1, \tag{A.4a}$$

$$\frac{p - p_1}{u - u_1} = \left(\frac{du}{dp}\right)^{-1}_{p_1} = (C_1)_w, \quad \text{for } \alpha_1 = 1, \tag{A.4b}$$

which is in agreement with the direct linearization of (3.5a) and (3.7a), which gives (3.10a) and (3.10b), respectively, which – in fact – already are the two families of linearized Poisson curves, with bulk densities ρ_0 and ρ_1 and speeds of sound c_0 and c_1 valid for all $(\alpha_0, \alpha_1) \in \{[0,1] \times [0,1]\}$.

A.3 Families of Hugoniot curves

In a Lagrangean formulation in which the shock wave is set still, across a shock connecting the pre-shock state (u_0, p_0) and the post-shock state $(u_{\frac{1}{2}}, p_{\frac{1}{2}})$, the flow is always from left to right (Figure 17a). Vice versa, across a shock connecting the pre-shock state (u_1, p_1) and the post-shock state $(u_{\frac{1}{2}}, p_{\frac{1}{2}})$, the flow is always from right to left (Figure 17b).

a. Shock wave connecting (u_0, p_0) and $(u_{1/2}, p_{1/2})$ b. Shock wave connecting (u_1, p_1) and $(u_{1/2}, p_{1/2})$

Figure 17: Shock waves in shock frame.

In the shock frame, the jump conditions corresponding with the situation of Figures 17a and 17b are, respectively

$$\begin{bmatrix} u \\ p \end{bmatrix} = m \begin{bmatrix} \frac{1}{\rho} \\ -u \end{bmatrix}, \tag{A.5a}$$

$$\begin{bmatrix} u \\ p \end{bmatrix} = m \begin{bmatrix} -\frac{1}{\rho} \\ u \end{bmatrix}, \tag{A.5b}$$

where m is the mass flow $|\rho u|$ through the shock wave. For a derivation of these shock relations in a Langrangean formulation, see [51], Section 62. From both (A.5a) and (A.5b) it follows

$$m = \sqrt{\frac{[p]}{-[1/\rho]}}. \tag{A.6}$$

Using (A.6), the above two jump conditions for momentum can be written as, omitting the subscripts for the post-shock quantities,

$$p - p_0 = -\sqrt{\frac{p - p_0}{\frac{1}{\rho_0} - \frac{1}{\rho}}}(u - u_0), \tag{A.7a}$$

$$p - p_1 = \sqrt{\frac{p - p_1}{\frac{1}{\rho_1} - \frac{1}{\rho}}}(u - u_1). \tag{A.7b}$$

With in equation (A.7a) the bulk densities $\rho_0 = \rho_0(\alpha_0, p_0)$ and $\rho = \rho(\alpha_0, p)$ according to (3.1b), (A.7a) determines one family of Hugoniot curves, one curve for each value of $\alpha_0 \in [0,1]$. Likewise, (A.7b) does for $\alpha_1 \in [0,1]$. Equations (A.7a) and (A.7b) are the shock analogies of the rarefaction equations (A.1a) and (A.1b). Working out (A.7a) and (A.7b) for general α_0 and α_1 on the basis of Tait's equation of state is tedious. As far as the nonlinear equations are concerned, here we also restrict ourselves to the specific case $\alpha_0 = \alpha_1 = 1$ (100% water in the left and right control volume). Elimination of the densities from (A.7a) and (A.7b) with Tait's equation of state yields after some rewriting

$$p - p_0 = -(C_0)_w \sqrt{\frac{1}{\gamma_w} \frac{\frac{p+B_w p_\infty}{p_0+B_w p_\infty} - 1}{1 - \left(\frac{p_0+B_w p_\infty}{p+B_w p_\infty}\right)^{\frac{1}{\gamma_w}}}}(u - u_0), \quad \text{for } \alpha_0 = 1, \tag{A.8a}$$

$$p - p_1 = (C_1)_w \sqrt{\frac{1}{\gamma_w} \frac{\frac{p+B_w p_\infty}{p_1+B_w p_\infty} - 1}{1 - \left(\frac{p_1+B_w p_\infty}{p+B_w p_\infty}\right)^{\frac{1}{\gamma_w}}}}(u - u_1), \quad \text{for } \alpha_1 = 1. \tag{A.8b}$$

Linearization of (A.8a) and (A.8b) around (u_0, p_0) and (u_1, p_1), respectively, yields

$$\frac{p - p_0}{u - u_0} = \left(\frac{du}{dp}\right)^{-1}_{p_0} = -(C_0)_w, \quad \text{for } \alpha_0 = 1, \tag{A.9a}$$

$$\frac{p - p_1}{u - u_1} = \left(\frac{du}{dp}\right)^{-1}_{p_1} = (C_1)_w, \quad \text{for } \alpha_1 = 1, \tag{A.9b}$$

which is identical to (A.4a) and (A.4b) (as it should because the Hugoniot curve and the Poisson curve through a point in state space are tangent to each other in that point).

Equations (A.7a) and (A.7b), which are valid for general α_0 and α_1, respectively, can also be linearized more directly. For that purpose, rewrite both equations as

$$p - p_0 = -\sqrt{\rho\rho_0}\sqrt{\frac{p - p_0}{\rho - \rho_0}}(u - u_0), \quad \rho_0 = \rho_0(\alpha_0, p_0), \quad \rho = \rho(\alpha_0, p), \quad \alpha_0 \in [0,1], \tag{A.10a}$$

$$p - p_1 = \sqrt{\rho\rho_1}\sqrt{\frac{p - p_1}{\rho - \rho_1}}(u - u_1), \quad \rho_1 = \rho_1(\alpha_1, p_1), \quad \rho = \rho(\alpha_1, p), \quad \alpha_1 \in [0,1]. \tag{A.10b}$$

Linearizing $\sqrt{\frac{p-p_0}{\rho-\rho_0}}$ as c_0, $\sqrt{\frac{p-p_1}{\rho-\rho_1}}$ as c_1, and taking $\sqrt{\rho\rho_0}$ and $\sqrt{\rho\rho_1}$ as ρ_0 and ρ_1, respectively, more directly gives the linear relations

$$\frac{p - p_0}{u - u_0} = -C_0, \quad C_0 = C_0(\alpha_0, p_0), \quad \alpha_0 \in [0,1], \tag{A.11a}$$

$$\frac{p - p_1}{u - u_1} = C_1, \quad C_1 = C_1(\alpha_1, p_1), \quad \alpha_1 \in [0,1]. \tag{A.11b}$$

A.4 Intermediate states

For the wave pairs sketched in Figure 15, the intermediate states $(u_{\frac{1}{2}}, p_{\frac{1}{2}})$ lie in or at the boundaries of the shaded quadrilaterals in Figures 18a–d. The specific state $(u_{\frac{1}{2}}, p_{\frac{1}{2}})$ is determined by the specific values α_0 and α_1. Note that due to the convexity of the Poisson curves, the linearized expressions are more sensitive to cavitation, in case of a double rarefaction, than the nonlinear expressions are. A double rarefaction in pure water is even more sensitive than a double rarefaction in pure air; compare $(u_{\frac{1}{2}}, p_{\frac{1}{2}})_{\alpha_0=1,\alpha_1=1}$ to $(u_{\frac{1}{2}}, p_{\frac{1}{2}})_{\alpha_0=0,\alpha_1=0}$ in Figure 18a.

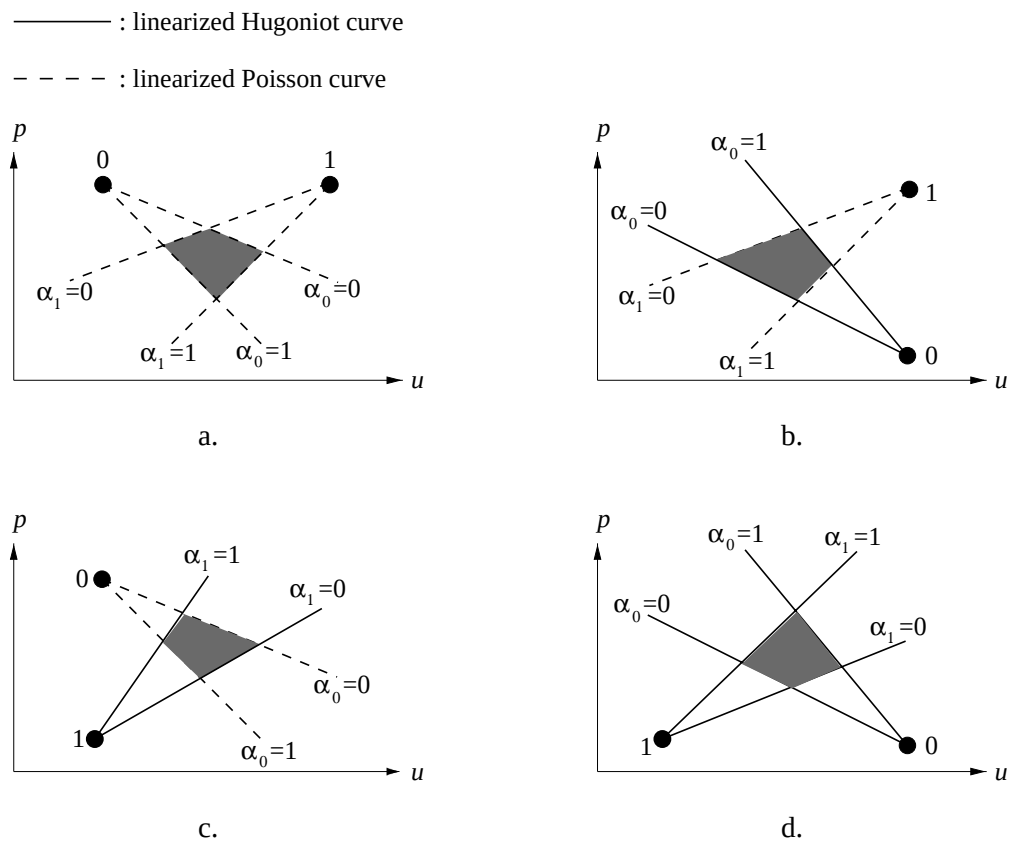

Figure 18: Families of linearized Poisson and Hugoniot curves in state space, two-fluid combinations a–d correspond with wave pairs in Figures 15a–d.

Table of Contents